Dalton Transactions

Accepted Manuscript

ROYAL SOCIETY OF CHEMISTRY

www.rsc.org/dalton

Highly efficient degradation of dye pollutants by Ce-doped MoO_3 catalyst at room temperature

Yujian Jin, Na Li, Haiqiu Liu, Xia Hua, Qiuying Zhang, Mindong Chen, Fei Teng *

Jiangsu Engineering Technology Research Centre of Environmental Cleaning Materials, Jiangsu Key Laboratory of Atmospheric Environment Monitoring and Pollution Control, Innovative Laboratory of Environment and Energy, School of Environmental Science and Engineering, Nanjing University of Information Science & Technology，219 Ningliu Road, Nanjing 210044, China

Abstract

In order to efficiently degrade organic pollutants via an easy operation way, Ce-doped MoO_3 (Ce(x)/MoO_3) samples are synthesized by a simple impregnation method. The samples are characterized by scanning electron microscope (SEM), X-ray diffraction (XRD), high-resolution transmission electron microscopy (HRTEM), selected area electron diffraction (SAED), nitrogen sorption isotherms and UV-vis diffused reflectance spectra (UV-DRS), total organic carbon (TOC), Infrared Spectroscopy (IR) and Mass Spectrometer (MS) analyses. Furthermore, we have mainly investigated, the degradations of different dyes pollutants by Ce(x)/MoO_3 samples, including cationic methylene blue (MB), anionic methyl orange (MO), neutral phenol, and MB-MO mixture dye. For single-component MB and MO dyes,

*Corresponding author. Email: tfwd@163.com (F. Teng); Phone/Fax: 0086-25-58731090

the highest degradation efficiencies are achieved by Ce(5)/MoO_3 and Ce(10)/MoO_3 samples, respectively. For MB-MO mixture dyes, the highest degradation efficiency of MB is achieved by Ce(10)/MoO_3 sample. It is surprising that the degradation efficiency of MB in MB-MO mixture dye solution is higher than that in single-component MB dye solution, which has been mainly ascribed to the promoting effect of MO. Moreover, a plausible degradation mechanism of dyes have been proposed and discussed. It should be noted that the degradation reaction is carried out at room temperature and normal atmospheric pressure, as well without light irradiation. As a result, this degradation reaction is obviously different from conventional thermally activated heterogeneous catalysis (or photocatalysis), in which thermal energy (or light irradiation) is indispensible; also different from sorption technology, in which the pollutants can not be degraded, but only be transformed from one phase to another one. Thus, the reported degradation reaction is a quite promising environmental cleaning technology, which could be widely applied in practice.

Keywords: Highly efficient degradation; Degradation reaction; Dye pollutant; Doption; Ce-doped molybdenum trioxide

1. Introduction

Due to severe harms to human health and ecosystem, the cleaning of dyestuff wastewater has aroused wide public concerns. Usually, stable polycyclic aromatic hydrocarbons are contained in organic dyes pollutants. Therefore, conventional physical methods can not effectively degrade these dyes pollutants. [1-7] For example, adsorption, ultra filtration, reverse osmosis and ion exchange can only transform the pollutants from wastewater to another phase, but can not degrade them.[3-6] On the other hand, dyes pollutants can be decompose completely by chemical methods. [7-10] Among them, photo catalysis that only needs abundant solar energy is a green environmental cleaning technology. However, many degradation reactions occur under ultraviolet radiation with a low utilization of solar energy; under visible light the degradation efficiencies are fairly low[10] which limits its applications in practices. Wet air oxidation (WAO) technology [11-12] has been applied in the degradation of pollutants. Nevertheless, the oxidation chemicals are usually needed; moreover, a high pressure (0.5-20 MPa) and a high temperature (175-320 °C) are necessary to maintain continuous progress of reaction.[12] This will significantly consumes fossil energy and increases the cost of equipment. Catalytic oxidation reaction is an efficient environmental cleaning technology for the removal of pollutants. Nevertheless, the catalytic reactions are usually carried out at high temperatures and/or high pressures, other than at room temperature and/or normal atmospheric pressure. Thus, heating and/or pressure-enduring equipment are/is usually needed. It is an energy-consumption and/or a high cost process. From energy-saving viewpoint, it is highly desirable to develop an efficient degradation reaction to completely decompose environmental pollutants, which can be operated at room temperature and normal

atmospheric pressure. To date, although some scholars have reported thermal catalytic degradations of environmental pollutants at room temperature,[13,14] even at the temperatures lower than room temperatures .[15] But three main disadvantages are obvious: i) non-precious metals oxides usually have no or fairly low activities at room temperatures, precious metals (such as Pt, Pd, Au)[13] are usually employed in room-temperature catalytic reactions. Therefore, the high cost and the limited resources of precious metals limit the widely applications in practices. ii) For the room-temperature catalytic reactions reported above, only simple small molecules (e.g., CO, HCHO, etc.) are selected as the target pollutants.[13,15] However, the dyes pollutants (e.g., MB, MO, etc.) usually have more stable, complex polycyclic aromatic structures, which is not easy to be degraded. iii) Conventional thermally catalytic reactions are usually carried out under gas/solid conditions. [13-15] Nevertheless, the dyes pollutants with high molecules weights have high evaporation pressures and usually exist in wastewater. Therefore, the degradation can not occur under conventional gas/solid conditions. As a result, it is still unknown whether these dyes pollutants can be degraded at room-temperature without light irradiation or not. Therefore, it is highly challengeable to degrade these toxic dyes pollutants using the efficient, inexpensive non-precious metals oxides catalysts.

Due to the wide applications in various fields, cerium and molybdenum oxides have caused researchers' concerns. For example, cerium can act as a fantastic oxygen storage and release reservoir through a facile mutual transformation of Ce^{4+}/Ce^{3+} under oxidation-deoxidation conditions. [17] Likewise, MoO_3-CeO_2 is an effective selective catalytic reduction (SCR) catalyst to remove nitrogen oxides (NO_x).[18,19] Also, V-Mo(W)/TiO_2 is one of the most widely commercially used SCR catalyst.[20] Furthermore, Ce/TiO_2, as a sorbent for elemental mercury (Hg^0) in simulated flue gas,

exhibits the advantages of both catalytic oxidation and oxygen storage.[17] To the best of our knowledge, however, only Zhao et al.[2,21] have used Ce/MoO_3 to catalytically degrade organic dyes at room temperature so far. Regrettably, they only reported the influences of doping amounts, temperature and pH value on the degradation of cationic Rhodamine B and Safranin-T dyes.[2,21] However, the catalytic mechanism at room temperature is still unclear. Furthermore, industrial wastewater often contains many different pollutants, therefore it also remain unknown its degradation performances for the other types of dyes pollutants. Herein, we have investigated the room-temperature degradation reactions for cationic methylene blue (MB), anionic methyl orange (MO), neutral phenol and MB-MO mixture dye, so as to demonstrate its feasibility in practical applications.

In this study, a simple impregnation-calcination method is employed to prepare Ce-doped MoO_3 catalysts. The degradation efficiencies of different type dyes have been mainly investigated at room temperature and normal atmospheric pressure. This contribution is aimed to bring a new concept to develop an energy-saving reaction for environmental cleaning.

2. Experimental Section

2.1. Catalyst preparation

All reagents were of analytical grade, purchased from Beijing Chemical Reagents Company of China and used without further purification.

MoO_3 samples. A simple hydrothermal method was used to prepare the sample. Typically, 0.5 mmol ammonium peramolybdate ($(NH_4)_6Mo_7O_{24}\cdot 4H_2O$) was firstly dissolved in 5 mL of distilled water. Then, 1.59 mL of 2.2 $mol\cdot L^{-1}$ HNO_3 solution was

added to the solution above under stirring. After stirring for 3 min, the solution was transferred into a 60-mL Teflon-lined stainless steel autoclave, and was then heated at 180 °C for 4 days. After hydrothermal treatment, the autoclave was cooled to room temperature naturally. Sequentially, a white precipitates was collected by centrifuging, and washed with distilled water and ethanol for three times, respectively. Finally, the sample was dried in an oven at 80 °C for 3 h.

Ce-doped MoO_3 (Ce(x)/MoO_3) samples. The samples were synthesized by wet impregnation and calcination methods while using the as-synthesized MoO_3 above as precursor. Typically, the as-synthesized MoO_3 powders above were impregnated in 20 mL of $Ce(NO_3)_3 \cdot 6H_2O$ solution. After impregnation, the samples were dried at 395 K for 3 h. The dried powders were then transferred into a muffle furnace to calcine in air. The samples were calcined at 473 K for 10 min and then 573 K for 3 h at a rate of 10 °C min^{-1}. To obtain Ce(x)/MoO_3 samples with different mass percentages of CeO_2, the concentration $Ce(NO_3)_3 \cdot 6H_2O$ solution is varied while 0.15 g of MoO_3 are used. Herein, the as-prepared Ce-doped MoO_3 catalysts are designated as Ce(x)/MoO_3, where x represents the nominal mass percentage of CeO_2 in Ce(x)/MoO_3.

2.2. Characterization

The crystal structures of the samples were determined by X-ray powder polycrystalline diffractometer (Rigaku D/max-2550VB), using graphite monochromatized Cu K_α radiation (λ= 0.154 nm), operating at 40 kV and 50 mA. The XRD patterns were obtained in the range of 10-80° (2θ) at a scanning rate of 5 °min^{-1}. The samples were characterized on a scanning electron microscope (SEM, Hitachi SU-1510) with an acceleration voltage of 15 keV. The samples were coated with 5-nm-thick gold layer before observations. The fine surface structures of the samples

were determined by high-resolution transmission electron microscopy (HRTEM, JEOL JEM-2100F) equipped with an electron diffraction (ED) attachment with an acceleration voltage of 200 kV. Surface areas and the pore sizes of the samples were calculated by the Brunauer-Emmett-Teller (BET) and Barret-Joyner-Halender (BJH) methods, respectively.

2.3. Degradation reaction

The catalytic activities of the catalysts were evaluated by the degradation reactions of single MB dye (5 mg L^{-1}), single MO dye (15 mg L^{-1}), MB (5 mg L^{-1})-MO(15 mgL^{-1}) mixture dye aqueous solution, and phenol (42.8 mg L^{-1}) ethanol-water solution, respectively. Herein, phenol was dissolved in an ethanol-water mixture (10 mgL^{-1}, $V_{ethanol}/V_{water}$=2/5), since phenol does not dissolve in water. All the reactions were performed at room temperature and normal atmospheric pressure, but without light irradiation.

Typically, 0.1 g of powders was suspended in 200 mL of dye solution under continuous magnetic stirring. During reaction, 3 mL of suspension was collected at a given interval time and centrifuged to remove the powders. The concentration of dye was determined by using UV–vis spectrophotometer.

3. Results and discussion

3.1. Characterization of the samples

Figure 1 shows SEM images of the samples. It can be observed from Figure 1(a,b) that the undoped MoO_3 sample is composed of six-prism-like micro-rods with the average lengths of 4-9 μm. Interestingly, these micro-rods form the grape

bunches-like assembles, and their surfaces are smooth without any micro-particles attached on. Figure 1(c-f) represents SEM images of Ce(*x*)/MoO_3 samples (x = 5, 10, 20 and 40). It is obvious that these samples show the irregular appearances, and the original well-organized MoO_3 grape bunches have been destroyed due to the high-temperature calcination. Compared with Figures 1(a,b), it is obvious that there exist some micro-particles on the prisms surfaces, the micro-particles attached on the surfaces become more and their agglomerations also become significant with the increase of Ce. This may indicate the formation of CeO_2.

The fine structures of the typical samples are further characterized by HRTEM. Figures 2a,b and e represent TEM images of *h*-MoO_3, Ce(*5*)/MoO_3 and Ce(*40*)/MoO_3 samples, respectively. Figure 2a shows that the sample is composed of tubular columns, which is consistent with the hexagonal structure of MoO_3 (*h*-MoO_3). It is well known that orthorhombic MoO_3 (α-MoO_3) has a distinctive layer structure and monoclinic MoO_3 (β-MoO_3) is metastable.[22] It has been reported that *h*-MoO_3 has excellent physical and chemical properties due to its one-dimensional (1D) tunnel structure.[23,24] Hexagonal MoO_3 is made up of the zigzag chains of MoO_6 octahedra by corner sharing, resulting in the formation of large 1D channels. Such channel structure is convenient for the doption of foreign ions or molecules.[23,24]. Figure 2e shows that there are numerous micro-particles attached on the micro-rods surfaces. Besides, the lattice spacings have been determined to be 0.27 and 0.31 nm for Ce(*5*)/MoO_3 (Figure 2c) and Ce(*40*)/MoO_3 (Figure 2f) samples, which correspond to the inter-plane distances of (200) and (111) of CeO_2, respectively. The results confirm the presence of CeO_2 (JCPDS No.43-1002). Furthermore, both diffraction rings and diffraction spots can be observed in SAED patterns for both Ce(*5*)/MoO_3 (Figure 2d) and Ce(*40*)/MoO_3 (Figure 2g) samples. In Figures 2d and S1(a) (Seeing Electronic

supporting information (ESI)), two diffraction spots and two diffraction rings are observed obviously. The distances from both diffraction spots to the center are determined to be 0.15 nm, corresponding to the inter-plane spacings of (430) of MoO_3; and the distances from the diffraction rings to the center are 0.12 nm and 0.19 nm, corresponding to the inter-plane spacings of (420) and (220) of CeO_2, respectively. In Figures 2(g) and S1(b) of ESI, the determined distances from the diffraction spots to the center are 0.15 nm and 0.12 nm, corresponding to the inter-plane spacings of (430) and (419) of MoO_3, respectively; and the distances from the diffraction rings to the center are determined to be 0.12 nm and 0.19 nm, corresponding to the inter-plane spacings of (420) and (220) of CeO_2, respectively. The results confirm the single-crystalline nature of *h*-MoO_3 and polycrystalline nature of CeO_2, also indicating the presence of superfluous CeO_2 on MoO_3 surfaces, besides the doption of Ce in MoO_3.[24,25]

Figure 3 presents XRD patterns of the samples. It can be observed that the main crystal phase in Ce(*40*)/MoO_3 sample is *h*-MoO_3 (JCPDS No. 21-0569); and that a weak diffraction peak of CeO_2 ($2\theta=28.38^o$) (JCPDS No. 65-5923) has appeared for Ce(*40*)/MoO_3 sample. However, no diffraction peaks of CeO_2 can be observed for the other samples, indicating that Ce may have doped into MoO_3 or highly dispersed on the surfaces of MoO_3. Further observed from Figure 3b and Figure S2 (ESI), an obvious peak shift of *h*-MoO_3 has occurred towards a lower 2θ angle with increasing CeO_2 content, indicating that the crystal cell of *h*-MoO_3 has expanded. Moreover, the peak shift is significant at $x=5$, while the peak shifts do not increase again at $x>5$, indicating that 5% may be the maximum doping amount of Ce. The average crystal size (D) of MoO_3 can be calculated using Scherrer equation (1) as follows.

$$D = k\lambda/(\beta\cos\theta) \quad [\ \beta = \sqrt{(B^2 - b^2)}\ ] \tag{1}$$

where B represents the full width of half maximum (FWHM), b represents the constant of FWHM, λ is the wavelength (λ = 0.154 nm) of Cu K_α radiation, k is the parameter of 0.89, θ is diffraction angle, and D is the average crystal size. Table 1 lists the D values calculated on base of the (210) diffraction peak at $2\theta = 25.79^o$. The average crystal size of h-MoO_3 increases with the doption of Ce(IV), and the largest crystal size of h-MoO_3 is 113.5 nm for Ce(*5*)/MoO_3. It is well known that Ce(IV) ion radius (0.087 nm) is larger than Mo(VI) ion radius (0.059 nm). Mohamed et al.[25] have reported that when Mo(VI) is introduced into CeO_2, the crystal size of CeO_2 decreases. It is reasonable that the crystal size of MoO_3 increases when Ce(IV) is doped into MoO_3.

BET areas, pore volumes, and pore sizes of the samples are summarized in Table 2. It is found that except for Ce(*5*)/MoO_3 (5.7 m^2g^{-1}) , the doped Ce(x)/MoO_3 samples have larger BET areas (20.0-35.4 m^2g^{-1}) than the undoped MoO_3 sample (8.2 m^2g^{-1}), but all the doped Ce(x)/MoO_3 samples have greatly smaller BET areas than pure CeO_2. Compared with that of pure MoO_3, the higher BET areas of Ce(x)/MoO_3 ($x \neq 5$) samples can be attributed to the presence of superfluous CeO_2 on MoO_3 surfaces, since CeO_2 particles have a large BET area (108.9 m^2g^{-1}). Additionally, Ce(20)/MoO_3 sample has a small extent increase could be resultant from the severe aggregation of CeO_2 particles. For the Ce(40)MoO_3, it may be that more CeO_2 could contribute the increase of the BET area. However, the lower BET area of Ce(*5*)/MoO_3 sample may indicate that all Ce(IV) ions have doped into MoO_3 channels, leading to the volumetric increase of crystal cell. Besides, the pore volume of Ce(x)/MoO_3 by and large increases with increasing the amount of Ce, accompanied by an irregular variation of pore size. This means that at a higher amount of cerium added, a

significant amount of ceria as the secondary phase may support on MoO_3 surfaces or exist as the form of free particles. The existing ceria particles lead to the increase of pore volume and the irregular variations of pore sizes.[26] Besides, combined with XRD figures, we nearly do not detect the diffraction peak of CeO_2; and we find that the XRD peaks of all the doped samples have shifted to a low 2theta angle. The peak shift of Ce(5)/MoO_3 is obvious; but with further increasing of Ce, the peak shifts does not increase significantly again. . This shows that the volume of crystal cell expand when CeO_2 was doped. However, if Ce(IV) ions doped into MoO_3, the value of average particles size will decrease instead, this has been proved by Mohamed, M. M. et.al.[25] But from our results of average crystal sizes (*D*) in Table 1, the value of average particles size of all the doped samples had increased clearly.

Thus, we think that the doption of Ce into MoO_3 predominates in our study, rather than the doption of Mo into ceria.

3.2. Degradation reactions of dyes pollutants

We have investigated the degradation reactions of dyes by Ce(*x*)/MoO_3 catalysts, in which cationic methylene blue (MB), anionic methyl orange (MO), MB-MO mixture dyes and neutral phenol are used as the probe molecules, respectively. Herein, their corresponding molecular structures are presented in Scheme 1. It should be noted that all the catalytic degradation reactions were carried out at room temperature and normal atmospheric pressure, but without light irradiation.

3.2.1. Catalytic degradation of cationic MB dye

Figures 4a and 4b present the degradation curves and reaction kinetic curves of MB dye by the catalysts, respectively. Their degradation efficiencies follow the order as follows: Ce(*5*)/MoO_3 > Ce(*40*)/MoO_3 > Ce(*10*)/MoO_3 > Ce(*20*)/MoO_3 > CeO_2 >

h-MoO_3. It shows that after reaction for 50 min, the degradation efficiency of MB reaches 89% over Ce(5)/MoO_3, but the pure MoO_3 or pure CeO_2 almost has no activity. It is obvious that the degradation performance of Ce(*x*)/MoO_3 catalyst has been greatly improved by the doption of Ce. Moreover, compared with the results reported by Chithambararaj et al.[24] the activity of Ce(5)/MoO_3 without light irradiation are 4.5 and 3 times higher than those of *h*-MoO_3 under UV light irradiation and under visible light irradiation, respectively. It should be noted that light irradiation or heating has not been used in our study. So it is an energy-saving process, which is highly desirable for us. Moreover, the apparent rate constants (k_a) can be calculated by the formula (2) as follows.

$$k_a = \ln(c_0/c) \quad (2)$$

where c_0 and c represent the initial concentration and the real-time concentration of dye, respectively. Table 3 summarizes the k_a values of the degradation reaction. It is found that the degradation rate of MB by Ce(5)/MoO_3 catalyst is 81.5 times higher than that by pure MoO_3. Typically, Figure 5 shows UV-vis absorption spectra of MB dye at different reaction times over Ce(5)/MoO_3 catalyst. The maximum absorption peak of MB locates at 665 nm, accompanied by a shoulder peak at 605 nm, which result from the monomeric (0–0 band) and dimeric (0–1 band) forms of MB, respectively.[27,28] It is obvious that both absorption peaks have not shifted with reaction time, indicating that MB has been effectively degraded.[24]

On base of the reference,[21] a possible reaction mechanism can be explained by Equations (3-5) as follows:

$$MoO_3 + RH \rightarrow R + H^+ + Mo_2O_5 \quad (3)$$

$$Mo_2O_5 + CeO_2 \rightarrow Ce_2O_3 + MoO_3 \quad (4)$$

$$Ce_2O_3 + 1/2\ O_2 \rightarrow CeO_2 \quad (5)$$

In the process, the dye molecules firstly adsorb on the surfaces of MoO_3; then they are activated and disassociated into the immediate (R), while Mo(VI) itself is reduced to Mo(V); further, Mo(V) is oxidized to Mo(VI) by the Ce(IV) again, while Ce(IV) itself is reduced to Ce(III). At last, Ce(III) is oxidized to Ce(IV) again by oxygen in air. The facile reciprocal transformation between Ce(IV) and Ce(III) leads to its good oxygen storage and release abilities. [17]

3.2.2. Catalytic degradation of anionic MO dye

The degradation reaction of anionic MO dye has also been carried out at room temperature and normal atmospheric pressure, as well without light irradiation. It is found that all the Ce(x)/MoO_3 samples have lower degradation activity for anionic MO dye. After 50 min, the highest removal efficiency (14.9%) of MO is achieved for Ce(20)/MoO_3 (Figure S3 of ESI). It should be noted that the degradation reaction has occurred surely, but not merely adsorption of MB, because the pure CeO_2 sample has the largest BET area, but the decrease of MO is fairly small. If only adsorption occurred, the pure CeO_2 sample should has the largest adsorption amount. Thus, the degradation reactions of MO were measured for 8 h (Figure 6a). First, the degradation curves of MO over Ce(20)/MoO_3 and Ce(10)/MoO_3 catalysts are almost overlapped, and after 8 h, 55% MO can be removed by them. Secondly, the removal rates of MO follow the order as follows: Ce(10)/MoO_3 ≈ Ce(20)/MoO_3 > Ce(40)/MoO_3 > Ce(5)/MoO_3 > CeO_2 > h-MoO_3 (Figure 6b, Table 3). It can be observed from Table 3 that the removal rates of MO dye by Ce(x)/MoO_3 samples (x=10 and 20) are 53 times as high as that by pure h-MoO_3. Typically, Figure 7 presents UV-vis absorption spectra of MO solution at different reaction times over Ce(10)/MoO_3 sample. The maximum absorption peak has not shifted, probably meaning that the degradation

reaction of MO dye ocurs. Besides, Table 3 shows that the doped Ce(x)/MoO_3 catalysts have the significantly improved degradation rates of both cationic MB and anionic MO, compared with pure CeO_2 or MoO_3. Moreover, cationic MB dye is obviously easier to remove than anionic MO dye, which may be relative to their different molecule structures and electrical properties. Herein, cationic MB molecules may be easier to be adsorbed, activated and degraded by Ce(x)/MoO_3 catalyst than MO. Moreover, MO has a relatively stable, symmetrical, conjugated molecular structure, but MB has a simple molecule structure with N=N bond (Scheme 1). It has been demonstrated that the N=N bond is easy to be degraded under light irradiation.[29] The real reason needs further research in future. Typically, we have also investigated the degradation of the neutral phenol by Ce(*40*)/MoO_3 catalyst (Figure S4). It is found that the absorption peak of phenol at 270 nm gradually becomes weaker and finally disappears with increasing reaction time, indicating that phenol also can be degraded by the catalysts under the same conditions.

3.2.3. Catalytic degradation of MB-MO mixture dye wastewater

Furthermore, Ce(x)/MoO_3 catalysts have been employed to degrade MB-MO mixture dye wastewater, with the aim at simulating practical wastewater that usually contains more than one pollutant. It can be observed from Figure 8a that after 50-min reaction, 65.5% of MB has been removed by Ce(*10*)/MoO_3 catalyst, which is the largest removal efficiency among the catalysts. For single MB wastewater, only 52% of MB has been degraded by the same catalyst after 50 min (Figure 4a). A higher removal efficiency of MB in the mixture dye solution is likely resultant from a promoting effect by MO, in which MO may have improved the adsorption of MB on the catalyst surface due to their different electrical properties. Such promoting effect

still remains unclear and needs further study in future. Besides, the reaction kinetic curves of MB in MB-MO mixture dyes are shown in Figure 8b, and their apparent reaction rates follow the orders as follows: Ce(10)/MoO_3 > Ce(5)/MoO_3 > Ce(40)/MoO_3 > Ce(20)/MoO_3. Further observed from UV-Vis absorption spectra (Figure 9), two new absorption peaks have appeared at 247 nm and 289 nm, respectively. We could merely assume that one or two new chemicals probably form after MB is mixed with MO. It is important that the newly-generated chemicals may also be degraded by our Ce(x)/MoO_3 catalysts. However, the new chemicals remain unknown to us, which needs further research.

Moreover, the apparent rate constants of single MB, single MO, and MB in MB-MO mixture dyes have been compared and summarized in Table 3. Compared with pure MoO_3 or pure CeO_2, Ce-doped catalysts have the greatly improved degradation rates. Compared with single MB dye, the degradation rates of MB in MB-MO mixture dye solution are higher. This catalysts have different degradation performances for different dyes, we think it may be associated with ionic potential of catalyst itself. We know that ionic potential is proportional to the ionic electrovalence while inversely proportional to the ionic radius.[30] therefore, Mo has the larger ionic potential than Ce, this means that Mo has stronger polarization ability than Ce. In this regard, it is easier for MoO_3 to form strong complex anion (such as MoO_3-OH^-), so the catalysts (Ce(5)/MoO_3) containing more MoO_3 relative to Ce(10)/MoO_3 can adsorb more cationic dye (MB).while CeO_2 will weaken the adsorption. Additionally, MoO_3 provide oxidation for dyes when CeO_2 act as a fantastic oxygen storage and release reservoir. Therefore, the right amount of CeO_2 and MoO_3 is very important for different types of pollutants, together with the influence of ionic potential, Ce(10)/MoO_3 rather than Ce(40)/MoO_3 or Ce(5)/MoO_3 show good performance for

MO degradation.

Herein, we can only make a preliminary inference, limited by our experiment conditions. In fact, this needs further studying in future.

In order to understand the degradation process, the degradation of MB over the Ce(5)/MoO_3 catalyst is typically characterized by TOC, Infrared Spectroscopy (IR) and Mass Spectrometer (MS).

The corresponding TOC result has been shown in Figure S5 of ESI. It can be observed that the MB dye has a declination trend with the time is 16%, but it does not reach a complete conversion to CO_2 + H_2O after 4 hours. Two possible reasons can be considered. One may be that more time is needed to complete the mineralization at room temperature; the other may be that the dye has been decomposed into small molecules.

Further, we have performed IR (Figure S6.). Before and after treatment, the IR spectra in region 4000–500 cm^{-1} of MB also demonstrate that the MB dye has been mineralized partly. Before degradation, O-H stretching vibration peak at 3438 cm^{-1} and C-H stretching vibration peak of CH_3- at 2925 cm^{-1} appear; the significant peak at 1607 cm^{-1} belongs to aromatic ring C–C stretching vibration; the peaks at 1491 cm^{-1} and 1331 cm^{-1} are resultant from to the –C=C– bond and C–N stretching vibrations, respectively; the peak at 1392 cm^{-1} is swinging vibration of C-H. In addition, the peak at 1135 cm^{-1} is resultant from the stretching vibration of C-S. After treatment by Ce(5)/MoO_3 for 4h, the peaks of 1607 cm^{-1}, 1491 cm^{-1}, 1392 cm^{-1} and 1331 cm^{-1} disappear, indicating the destruction of three hexa-atomic rings or aromatic rings; the newly appeared peaks at 2366 cm^{-1}, 2361 cm^{-1} and 710 cm^{-1} may be attributed to the vibration of HCO_3^- anion, and also the peak at 1640 cm^{-1} is resultant from the vibration of C=O in HCO_3^- anion. Therefore, we could draw a conclusion that the

skeleton structure of benzene ring has been completely destroyed.

Besides, from the UV–vis absorption spectra of MB solution (Figure S7.), we can not observe the characteristic absorption peak after degradation.

Moreover, Figure S8 shows the MS spectra after degradation. We can find that after removing the background, an obvious peak with the molecular mass of 95.12 appears. Combined with IR analysis, we can preliminary inference it can be attributed to the small molecules containing C and H atoms, but not containing cyclic structure.

Based on the analysis results, this catalyst can degrade dyes into HCO_3^- or CO_3^{2-} and small molecules; moreover, benzene ring has been decomposed.

To conclude, the catalyst can be used to decolorize or degrade the dye, although the dye has not been completely mineralized into CO_2 and H_2O. It should note that the formed small molecules are needed to be further determined in future.

In conclusion, compared with conventional thermally activated heterogeneous catalysis or conventional photocatalysis, the degradation reaction is carried out without heating or light irradiation, respectively. As a result, this novel reaction does not consume an extra fossil fuel or need optical system to provide light energy. Hence, it is an energy-saving, low-cost reaction. This contribution is aimed to bring the innovative concept and protocol for the design of zero-energy-consumption environmental cleaning material and technology, which is highly desirable for us to be widely applied in practice.

3.3 Conclusions

The dyes pollutants can be efficiently degraded by Ce-doped MoO_3 catalysts and MB dye in MB-MO mixture dye can be degraded more efficiently than single MB dye, which is mainly resultant from their synergetic effect of adsorption and/or degradation.

Most importantly, the degradation reactions can be carried out without needing heating or light irradiation, compared with conventional thermally activated catalysis or photocatalysis. This contribution could bring an innovative concept to develop a zero-energy-consumption reaction for environmental cleaning technology.

Acknowledgements

This work is financially supported by National Science Foundation of China (21377060, 21103049), Six Talent Climax Foundation of Jiangsu (20100292), Jiangsu Science Foundation of China (BK2012862), Jiangsu Province of Academic Scientific Research Industrialization Projects (JHB2012-10, JH10-17), the Key Project of Environmental Protection Program of Jiangsu (2013016, 2012028), the Project Funded by the Science and Technology Infrastructure Program of Jiangsu (BM2013139, 201380277), the Project of Foreign Culture and Education Expert (N0502001003), A Project Funded by the Priority Academic Program Development of Jiangsu Higher Education Institutions (PAPD), and Jiangsu Province Innovation Platform for Superiority Subject of Environmental Science and Engineering, the Project Sponsored by SRF for ROCS, SEM (2013S002), “333” Outstanding Youth Scientist Foundation of Jiangsu (2011-2015).

References

(1) Meshko, V.; Markovska, L.; Mincheva, M.; Rodrigues, A. E. Adsorption of basic dyes on granular activated carbon and natural zeolite. *Water Res.,* 2001, 35 (14), 3357-3366.

(2) Zhao, S.; Li, J. Z; Wang, L.; Wang, X. H. Degradation of rhodamine B and safranin-T by MoO_3:CeO_2 nanofibers and air using a continuous mode. *Clean–Soil, Air, Water*, 2010*, 38* (3), 268-274.

(3) Konstantyinou, I. K.; Albanis, T. A. TiO_2-assisted photocatalytic degradation of azo dyes in aqueous solution: kinetic and mechanistic investigations. A review, *App. Catal. B: Environ*., 2004, 49, 1-14.

(4) Tang, W. Z.; An, H. UV/TiO_2 photocatalytic oxidation of commercial dyes in aqueous solutions. *Chemosphere*, 1995, 31 (9), 4157-4170.

(5) Kuo, W. S.; Ho, P. H. Solar photocatalytic decolorization of methylene blue in water. *Chemosphere*, 2001, 45 (1), 77-83.

(6) Galindo, C.; Jacques, P.; Kalt, A. Photo-oxidation of the phenylazonaphthol AO_{20} on TiO_2: kinetic and mechanistic investigations. *Chemosphere*, 2001, 45 (6), 997-1005.

(7) Xing, Z.; Zhou, W.; Du, F.; Qu, Y.; Tian, G. H.; Pan, K.; Tian, C. G.; Fu, H. G. A floating macro/mesoporous crystalline anatase TiO_2 ceramic with enhanced photocatalytic performance for recalcitrant wastewater degradation. *Dalton Trans*., 2014, 43 (2), 790-798.

(8) Ahmad, M.; Ahmed, E.; Hong, Z. L.; Ahmed, W.; Elhissi, A.; Khalid, N. R. Photocatalytic, sonocatalytic and sonophotocatalytic degradation of Rhodamine B

using ZnO/CNTs composites photocatalysts. *Ultrason. Sonochem*., 2014, 21 (2), 761-773.

(9) Tayade, R. J.; Natarajan, T. S.; Bajaj, H. C. Photocatalytic degradation of methylene blue dye using ultraviolet light emitting diodes. *Ind. & Eng. Chem. Res.*, 2009, 48 (23), 10262-10267.

(10) Yang, X. F.; Cui, H. Y; Li, Y.; Qin, J. L.; Zhang, R. X.; Tang, H. Fabrication of Ag_3PO_4-Graphene Composites with Highly Efficient and Stable Visible Light Photocatalytic Performance. *ACS Catal.*, 2013, 3 (3), 363-369.

(11) Neri, G.; Pistone, A.; Milone, C.; Galvagno, S. Wet air oxidation of p-coumaric acid over promoted ceria catalysts. *Appl. Catal. B: Environ*., 2002, 38 (4), 321-329.

(12) Zhang, X. W.; Wang, Y. Z.; Li, G. T.; Qu, J. H. Oxidative decomposition of azo dye C.I. Acid Orange 7 (AO7) under microwave electrodeless lamp irradiation in the presence of H_2O_2. *J. Hazard. Mater*., 2006, 134 (1), 183-189.

(13) Zhang, C. B; He, H.; Tanaka, K. I. Catalytic performance and mechanism of a Pt/TiO_2 catalyst for the oxidation of formaldehyde at room temperature. *Appl. Catal. B: Environ*., 2006, 65 (1), 37-43.

(14) Hu, Z. Y; Boiadjiev, V.; Thundat, T. Nanocatalytic spontaneous ignition and self-supporting room-temperature combustion. *Energ. & Fuel*, 2005, 19 (3), 855-858.

(15) Nagase, K.; Zheng, Y.; Kodama, Y.; Kakuta, J. Dynamic study of the oxidation state of copper in the course of carbon monoxide oxidation over powdered CuO and Cu_2O. *J.. Catal.*, 1999, *187* (1), 123-130.

(16) Xie, X.W.; Li, Y.; Liu, Z. Q.; Haruta, M., & Shen, W. J. Low-temperature oxidation of CO catalysed by Co_3O_4 nanorods. *Nature*, 2009, 458 (7239), 746-749.

(17) Zhou, J. S.; Hou, W. H.; Qi, P.; Gao, X.; Luo, Z. Y.; Cen, K. CeO_2-TiO_2 Sorbents for the Removal of Elemental Mercury from Syngas. *Environ. Sci. & Technol.*, 2013, 47 (17), 10056-10062.

(18) Li, J.; Liu, X. H. Preparation and characterization of α-MoO_3 nanobelt and its application in supercapacitor. *Mater. Lett.*, 2013, 112, 39-42.

(19) Lietti, L.; Ramis, G.; Berti, F. Chemical and mechanistic aspects of the selective catalytic reduction of NO_x by ammonia over oxide catalysts: A review. *Appl. Catal. B: Environ*., 1998, 18 (1), 1-36.

(20) Peng, Y.; Qu, R. Y.; Zhang, X. Y.; Li, J. H. Relationship between structure and activity of MoO_3-CeO_2 catalysts for NO removal: influences of acidity and reducibility. *Chem. Commun*., 2013, 49, 6215-6217.

(21) Li, W.; Zhao, S.; Qi, B.; Du, Y.; Wang, X. H.; Huo, M. X. Fast catalytic degradation of organic dye with air and MoO_3: Ce nanofibers under room condition. *Appl. Catal. B: Environ*. 2009, 92 (3), 333-340.

(22) Gao, B.; Fan, H. Q.; & Zhang, X. J. Hydrothermal synthesis of single crystal MoO_3 nanobelts and their electrochemical properties as cathode electrode materials for rechargeable lithium batteries. *J. Phys. Chem. Solids*, 2012,*73* (3), 423-429.

(23) Chithambararaj, A.; Sanjini, N. S.; Bose, A. C.; Velmathi, S. Flower-like hierarchical *h*-MoO_3: new findings of efficient visible light driven nano photocatalyst for methylene blue degradation. *Catal. Sci. Technol*. 2013, 3 (5), 1405-1414.

(24) Dhage, S. R.; Hassan, M. S.; Bong Yang, O. Low temperature fabrication of hexagon shaped *h*-MoO_3 nanorods and its phase transformation. *Mater. Chem*. 2009, 114 (2), 511-514.

(25) Mohamed, M. M.; Katib, S. M. A. Structural and catalytic characteristics of MoO_3/CeO_2 catalysts: CO oxidation activity. *Appl. Catal. A: Gen*. 2005, 287 (2), 236-243.

(26) Hua, X. Y.; Zhou, J. S.; Li, Q.; Luo, Z. Y.; Cen, K. F. Gas-phase elemental mercury removal by CeO_2 impregnated activated coke. *Energ. & Fuel* 2010, 24 (10), 5426-5431.

(27) Pourahmad, A.; Sohrabnezhad, S. A cost effective and sensitive method for the determination of ammonia concentration in nanocrystal mordenite. *Int. J. Nano. Dim.*, 2010, 1 (2), 143-152.

(28) Cenens, J.; Schoonheydt, R. A. Visible spectroscopy of methylene blue on hectorite, laponite B, and barasym in aqueous suspension. *Clays Clay Miner.*, 1988, 36 (3), 214-224.

(29) Rauf, M. A.; Meetani, M. A.; Hisaindee, S. An overview on the photocatalytic degradation of azo dyes in the presence of TiO_2 doped with selective transition metals. *Desalination*., 2011, 276, 13-27.

(30) Shafir, D.; Fabre, B.; Higuet, J.; Soifer, H.; Dagan, M.;Descamps, D.; Mairesse, Y.; et al. Role of the ionic potential in high harmonic generation. *Phys. Rev. lett.*. 2012, *108* (20), 203001.

Title list of Tables and Figures

mixture solution over Ce(x)/MoO_3 samples: 200 mL aqueous solution containing 5 mgL^{-1} MB and 15 mgL^{-1} MO

Figure 9. UV-vis absorption spectra of MB-MO mixture dye over Ce(10)/MoO_3 at different reaction times

Table 1

The average crystal sizes (D) of Ce(x)/MoO_3 samples

Samples	[1] B (rad)	[2] b (rad)	[3] θ (rad)	[4] D (nm)
Pure MoO_3	3.87×10^{-3}	1.74×10^{-3}	0.3968	43.0
Ce(5)/MoO_3	2.18×10^{-3}	1.74×10^{-3}	0.3957	113.5
Ce(10)/MoO_3	2.22×10^{-3}	1.74×10^{-3}	0.3947	108.7
Ce(20)/MoO_3	2.67×10^{-3}	1.74×10^{-3}	0.3942	74.4
Ce(40)/MoO_3	2.32×10^{-3}	1.74×10^{-3}	0.3938	97.3

[1] B: Full width at half of maximum peak (FWHM); [2] b: Constant; [3] θ: Diffraction angle; [4] D: calculated by Scherrer equation

Table 2

Texture properties of pure MoO_3, pure CeO_2 and Ce(x)/MoO_3 samples

Samples	[a] Surface area (m^2/g)	[b] Pore volume (cm^3/g)	[b] Pore diameter (nm)
Pure MoO_3	8.2	9.646×10^{-3}	3.059
Pure CeO_2	108.9	2.736×10^{-1}	9.597
Ce(5)/MoO_3	5.7	1.360×10^{-2}	1.936
Ce(10)/MoO_3	20.0	4.819×10^{-2}	19.110
Ce(20)/MoO_3	14.6	4.445×10^{-2}	3.832
Ce(40)/MoO_3	35.4	1.181×10^{-1}	7.756

[a] Surface area, calculated by the Brunauer-Emmett-Teller(BET) method; [b] Pore volume and pore diameter, calculated by the Barrett-Joyner-Halenda (BJH) method

Table 3

Apparent reaction kinetic constants (k_a) of dye over Ce(x)/MoO_3 catalysts

Samples	k_a (Single MB dye) (min^{-1})	k_a (MB in mixture dye) (min^{-1})	k_a (Single MO dye) (h^{-1})
Pure MoO_3	2.129×10^{-4}	/	0.00193
Pure CeO_2	5.596×10^{-4}	/	0.00652
Ce(5)/MoO_3	0.04263	0.00856	0.03807
Ce(10)/MoO_3	0.01241	0.01712	0.10150
Ce(20)/MoO_3	0.00691	0.00573	0.09923
Ce(40)/MoO_3	0.01798	0.01260	0.08767

Figure 1

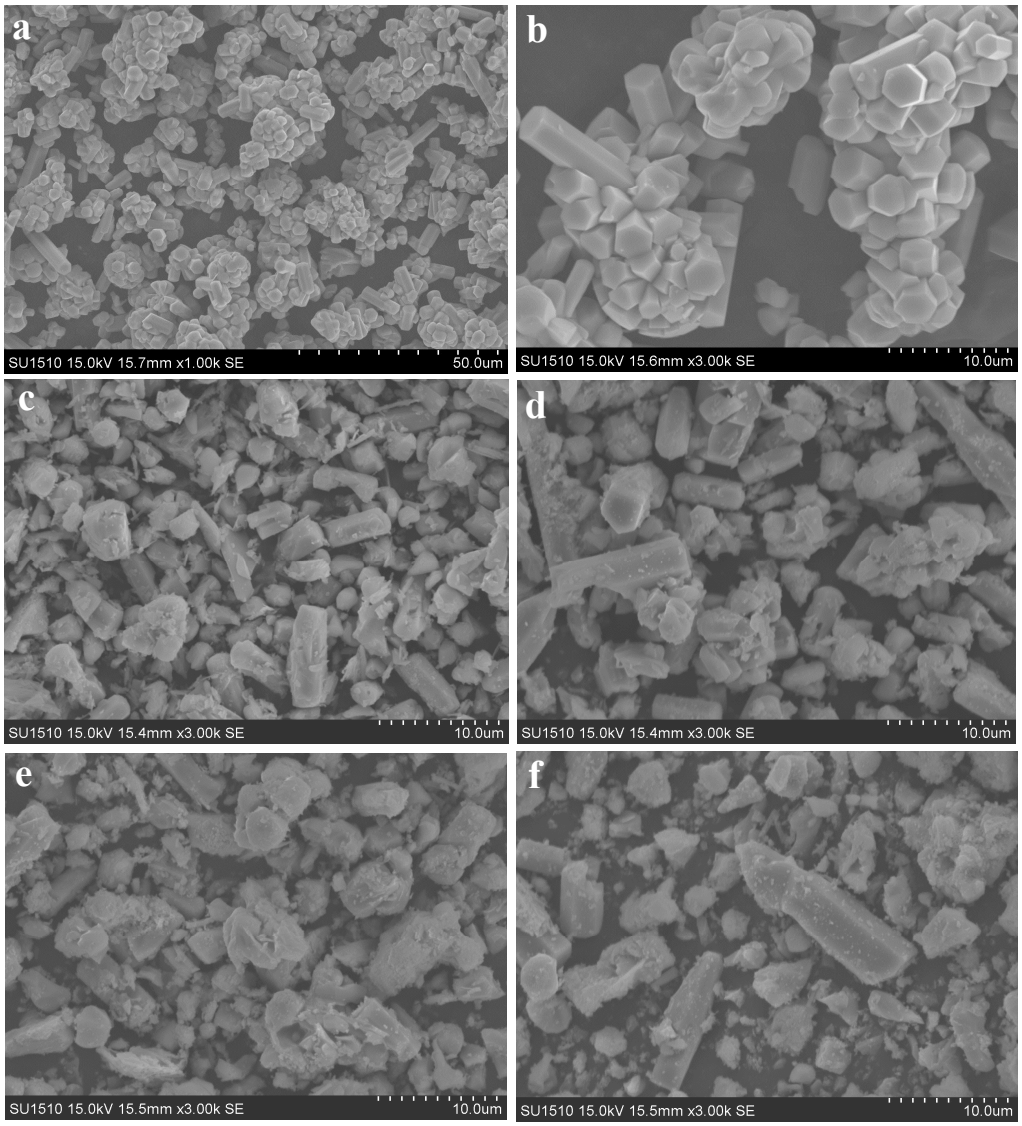

Figure 2

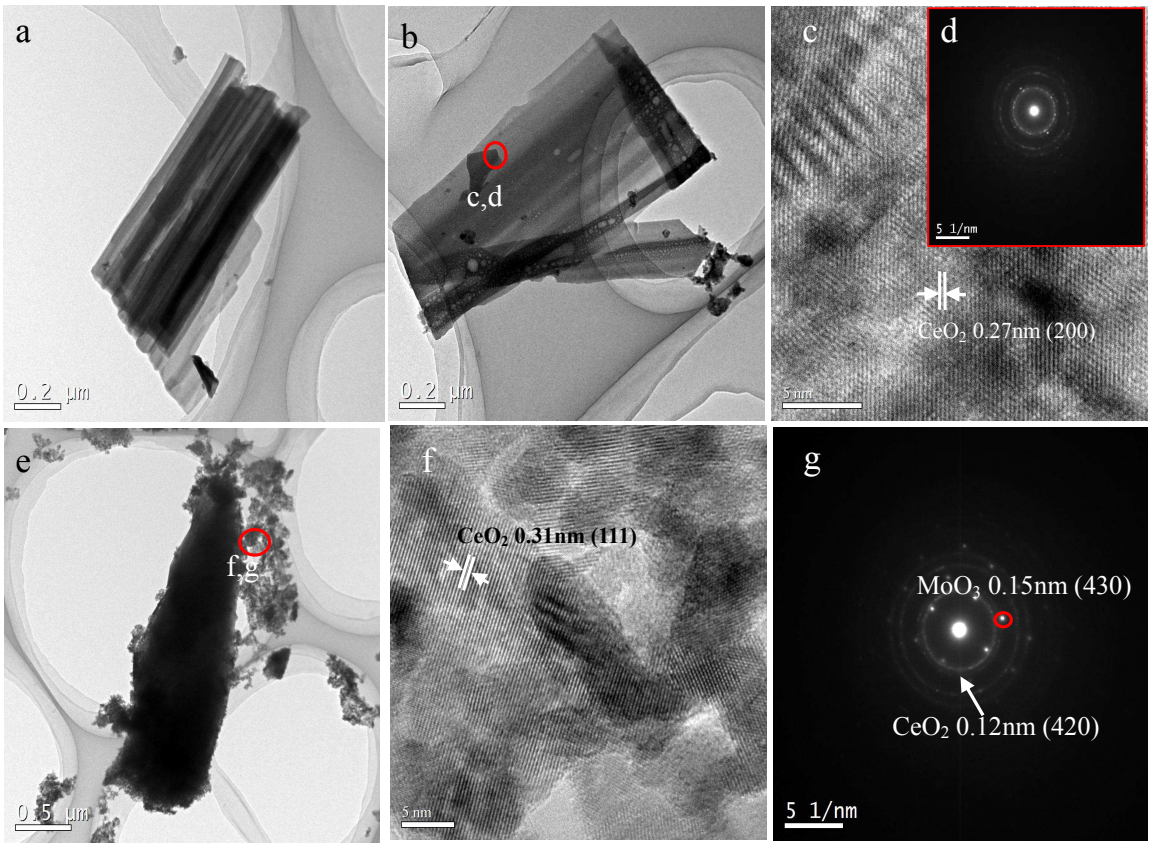

Figure 3

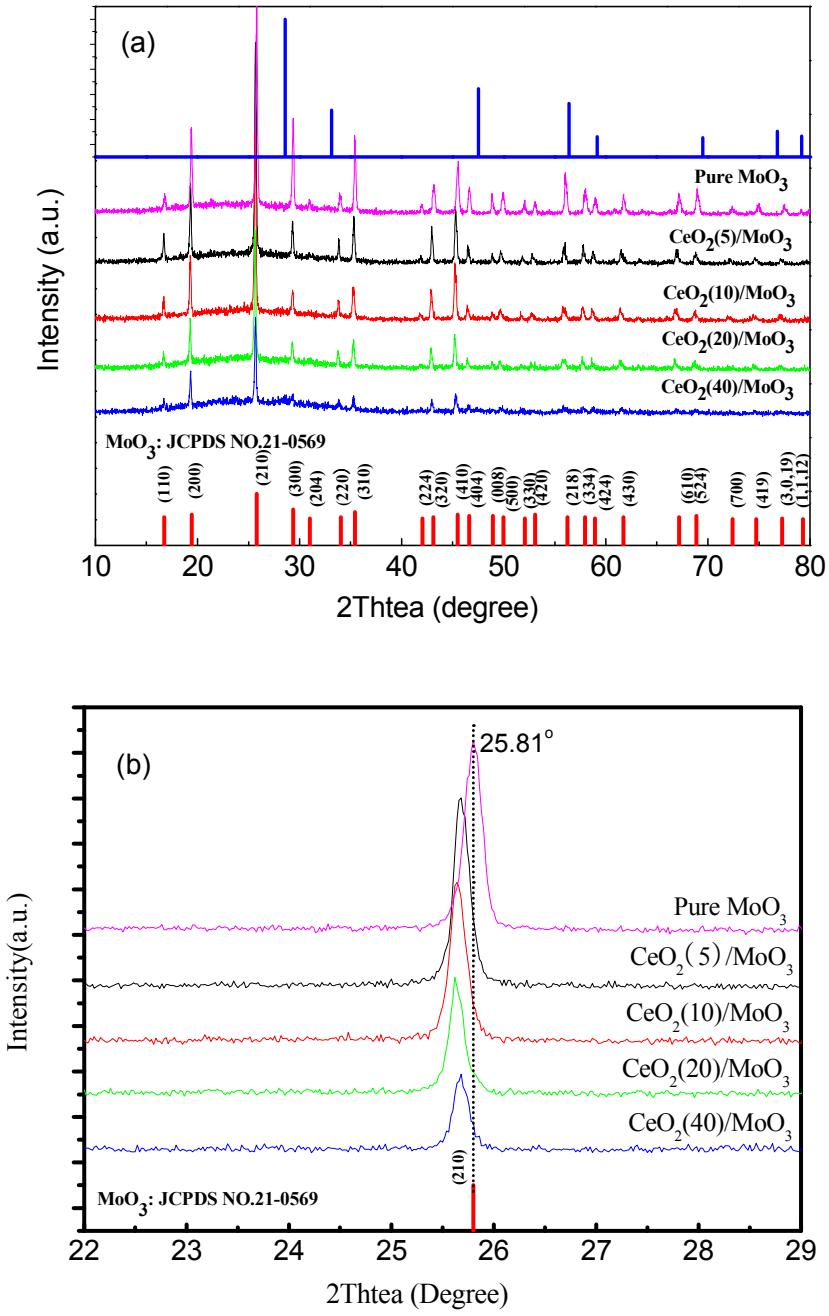

Scheme 1

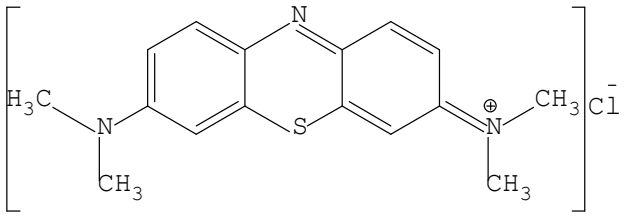

(a) MB

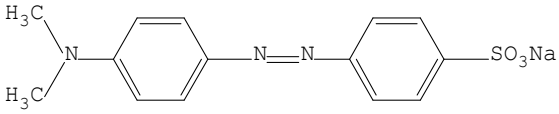

(b) MO

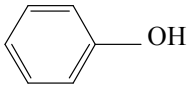

(c) Phenol

Figure 4

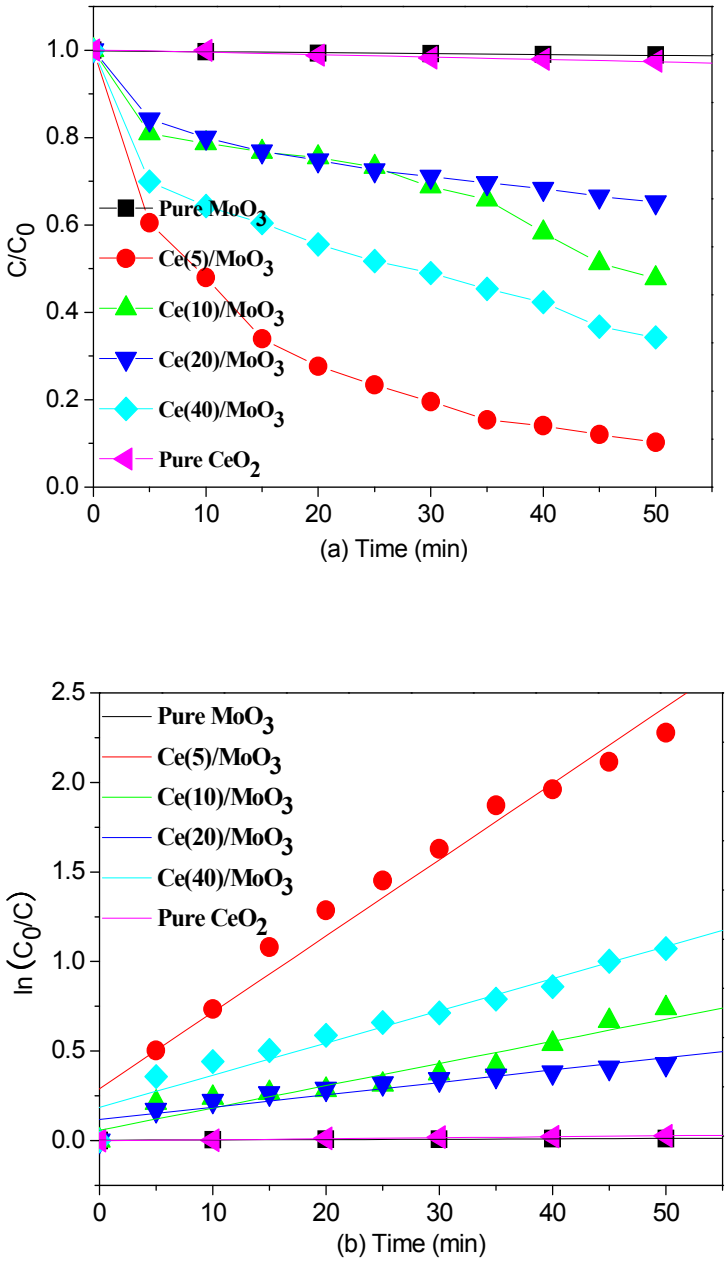

Figure 5

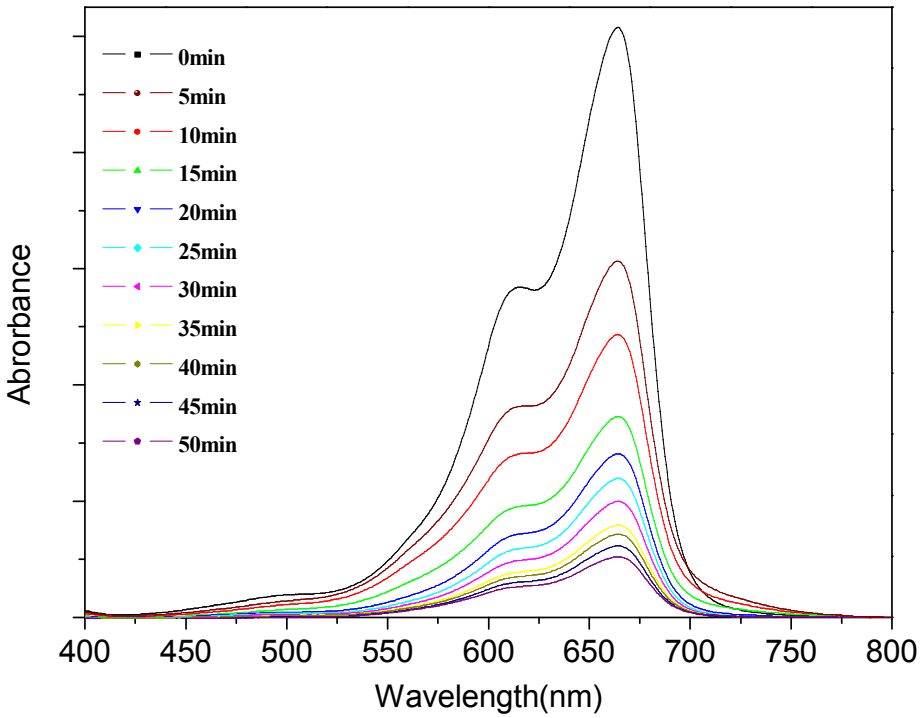

Figure 6

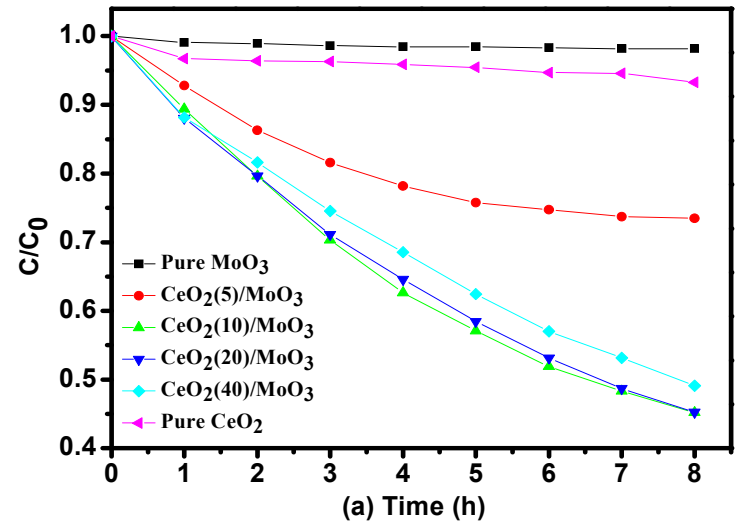

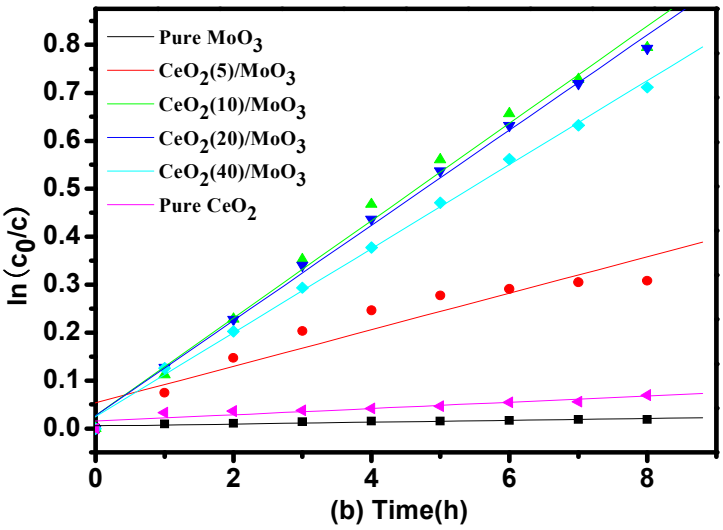

Figure 7

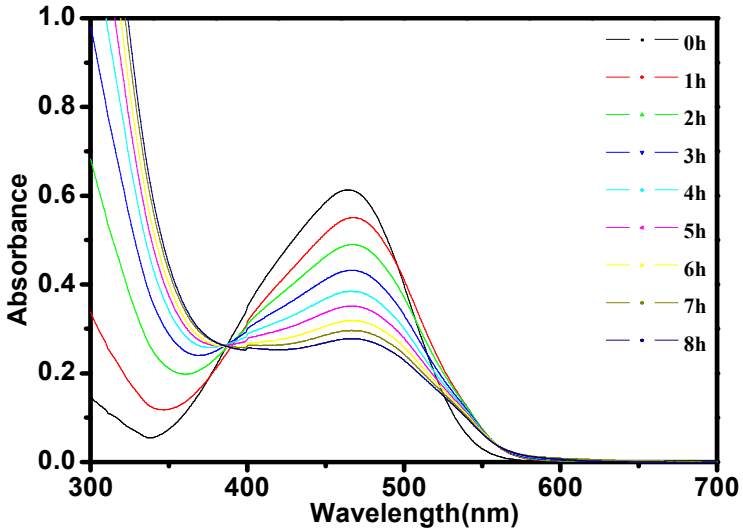

Figure 8

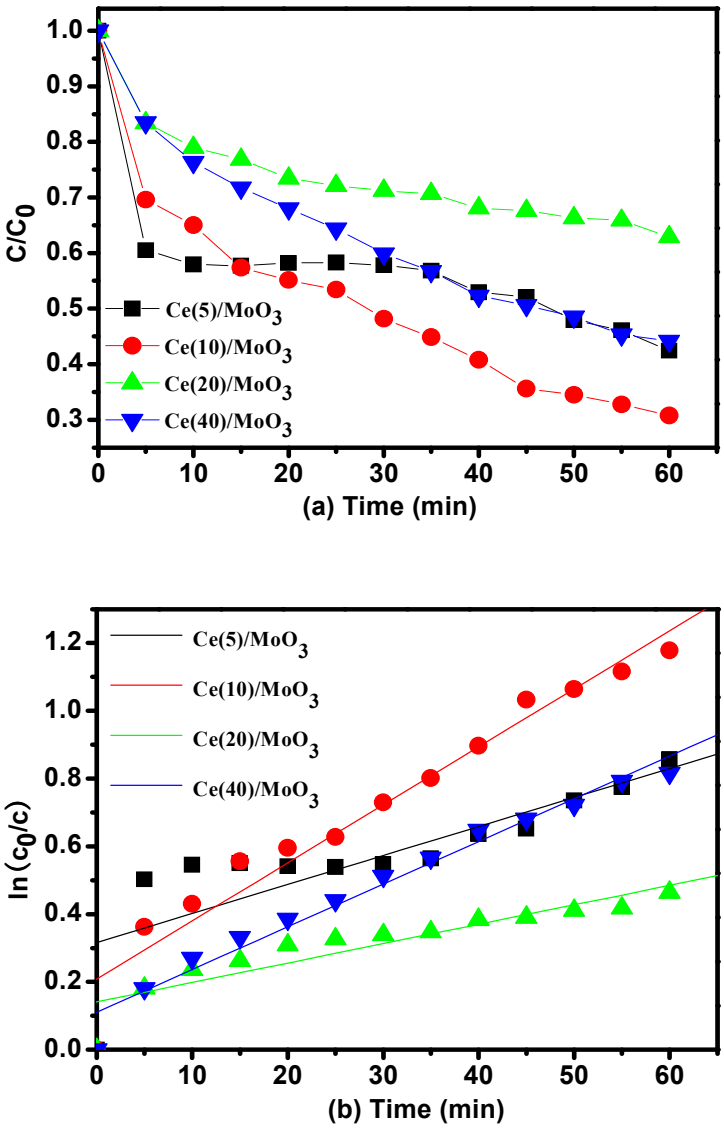

Figure 9

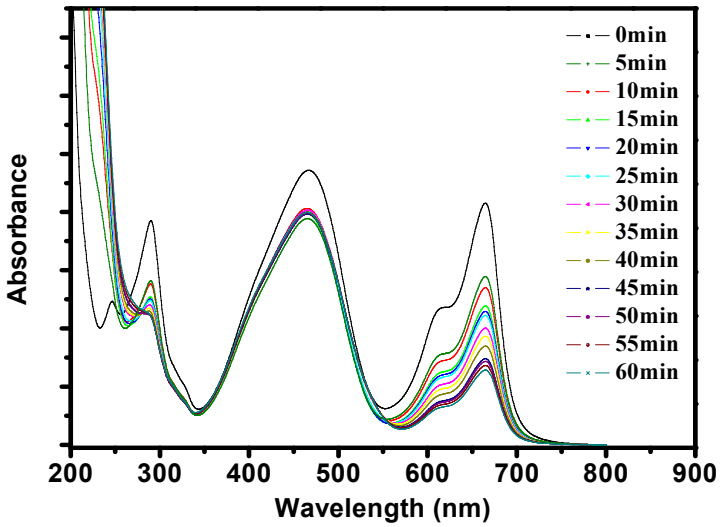

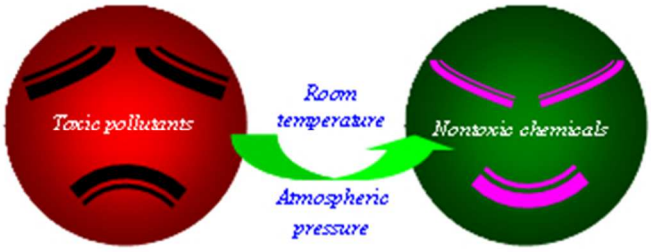

A novel energy-saving degradation reaction for dyes pollutants over Ce-doped MoO3 catalyst
76x29mm (120 x 120 DPI)